Renewable Energy 209 (2023) 1–9

Contents lists available at ScienceDirect

Renewable Energy

journal homepage: www.elsevier.com/locate/renene

An assessment of the scalings for the streamwise evolution of turbulent quantities in wakes produced by porous objects

Elizabeth H. Lingkan, Oliver R.H. Buxton *

Department of Aeronautics, Imperial College London, London, SW7 2AZ, UK

ARTICLE INFO

Keywords:
Turbulent wakes
Dissipation scaling
Cumulative turbulence intensity
Wake modelling

ABSTRACT

Experimental results are presented for the evolution of three turbulent quantities in the wake of a porous object, analogous to a wind-turbine wake. These are the mean velocity deficit, the turbulence intensity, and the characteristic wake width. It is noted that characteristic wake widths can be defined both in terms of the mean velocity deficit profile and the profile of turbulence intensity. Both definitions of wake width are observed to grow linearly, although not at the same rate, with that defined by turbulence intensity growing more rapidly than velocity deficit. The streamwise scaling of both wake width, and velocity deficit is found to conform to a non-equilibrium dissipation scaling in which the dissipation rate within the wake is out of equilibrium with the inter-scale energy flux within the mean cascade of turbulent kinetic energy. The cumulative effect of turbulence intensity produced by N upstream porous objects is also considered. It is shown that when the object spacing is sufficiently large that the wake-added turbulence decays substantially only consideration of the most immediately upstream wake is important. Contrastingly, when the spacing between adjacent objects is small then summing the contributions from all upstream wakes in the array is necessary.

1. Introduction

The wake of a wind turbine is well-characterised as a region of decreased wind velocity and increased turbulence which leads to a reduction in the power output and an increase in fatigue stresses of turbines situated within the wake of an upstream machine [1–3]. Predicting the spreading rates of turbulent wakes is thus vitally important to the process of designing optimal layouts for future wind farms, seeking to maximise overall power production whilst accounting for the structural and mechanical life of the turbines/components. Much of the analysis accounting for the spreading of turbulent wind-turbine wakes has only considered the highly simplified case of a non-turbulent background, whilst in reality wind turbines are situated within either the wake of an upstream machine or are exposed directly to the atmospheric boundary layer, both of which are turbulent environments. Higher levels of turbulence in the incoming flow into a wind turbine are known to increase the wake recovery rate due to an enhancement of the mixing processes [4]. It is thus vital to model the development (with downstream distance) of turbulent statistics, such as turbulence intensity, within wind-turbine wakes in future analytical wake models since the development of subsequent wakes will be affected by the turbulent inflow produced by upstream wakes.

Analytical (or "engineering") wake models are extensively used within the wind energy industry for the purposes of wind-farm design and control due to their relatively low complexity and computational cost [5,6]. Gaussian-type models are among the most commonly applied analytical wake models and were developed based on experimental and computational observations of wind-turbine wakes which identified that after some distance downstream, the mean velocity profile of the wake develops a self-similar, Gaussian profile—even under the conditions of turbulent boundary layer inflow [2,7]. These models rely on the common assumption that the wake grows *linearly* with a rate k that is a function of the incoming turbulence intensity to the turbine, I_0. As the wake growth determines the velocity recovery in the wake, accurate modelling of turbulence intensity between rows of turbines is therefore crucial for accurate velocity and power predictions of an array of turbines.

There have been numerous attempts in literature to model the turbulence intensity added by a turbine, I_+. Most commonly this is modelled as a constant value distributed across the whole wake corresponding to the peak turbulence intensity induced by the turbine. Crespo and Hernandez [1] developed the following expression by fitting to the results from RANS simulations of a single turbine wake

$$I_+ = 0.73\left(0.5\left(1-\sqrt{1-C_T}\right)\right)^{0.8325} I_0^{0.0325}(x/D)^{-0.32} \quad (1)$$

where C_T is the turbine's thrust coefficient, D is the turbine's rotor diameter, and x is the streamwise distance from the turbine. Frandsen

* Corresponding author.
E-mail address: o.buxton@imperial.ac.uk (O.R.H. Buxton).

https://doi.org/10.1016/j.renene.2023.03.101
Received 17 August 2022; Received in revised form 13 March 2023; Accepted 22 March 2023
Available online 24 March 2023

[8] developed a model which characterises I_+ as a function of C_T and the downstream distance only

$$I_+ = \left(c_1 + c_2 \frac{(x/D)}{\sqrt{C_T}} \right)^{-1} \tag{2}$$

where $c_1 = 1.5$ and $c_2 = 0.8$. More recently, Ishihara and Qian [9] developed a model that takes into account the spatial distribution of the turbulence intensity in the wake, i.e. $I_+ = I_+(x, y)$, by modelling a double-Gaussian profile

$$I_+ = \frac{1}{d + e(\frac{x}{D}) + f(1 + \frac{x}{D})^{-2}} \times \left[k_1 \exp\left(-\frac{(y - \frac{D}{2})^2}{2\sigma^2} \right) + k_2 \exp\left(-\frac{(y + \frac{D}{2})^2}{2\sigma^2} \right) \right] \tag{3}$$

where

$$k_1 = \cos^2(\pi/2 \cdot (r/D - 0.5)); \quad k_2 = \cos^2(\pi/2 \cdot (r/D + 0.5))$$

and d, e and f are constants dependent on C_T and I_0:

$$d = 2.3C_T^{-1.2}; \qquad e = 1.0I_0^{0.1}; \qquad f = 0.7C_T^{-3.2}I_0^{-0.45}$$

and $\sigma = \sigma(x)$ is the representative wake width (modelled with a linear spreading rate, i.e. $\sigma = kx/D + \text{const.}$). An important observation here is the different axial scalings, i.e. differing exponent α for $I_+ \sim x^\alpha$, for the three different models presented above which depicts the physical inconsistency in the available models. This can become particularly important in large wind farms, extending over large distances, which are becoming ever more common. Presently, the available engineering models for wind-turbine wakes are built upon empirical correlations established under a specific range of conditions, thus it is not surprising to find such a range of scalings used. The purpose of this study is thus to continue building the foundation of evidence for establishing a physics-based and theoretically-grounded model for the evolution of turbulent quantities in arrays of wind turbines which will then inform more accurate, and hopefully universally-applicable, tools for wind-farm development. Despite the high volume of research into the modelling of wind-turbine wakes, the literature on analytical wake models for turbulent quantities has been less rigorous — thus in the present study, there is a larger focus on investigating the evolution and combination of turbulent quantities from multiple turbine wakes.

Gaussian wake models make an implicit assumption that wakes behave in such a self-similar fashion in order to preserve the functional form of the wake's profile. Previous studies on self-similar axisymmetric turbulent wakes have yielded predictions on the axial scaling of the maximum (centreline) mean velocity deficit, Δu_C, and the wake width r_w with downstream distance x. Classically, this was predicted in George [10] to be $\Delta u_C \sim x^{-2/3}$ and $r_w \sim x^{1/3}$ for high Reynolds number flows past solid, axisymmetric objects. This theory was developed by using a closure on the self-similar form of the dissipation rate within the wake. In particular, the classical closure

$$\varepsilon = C_\varepsilon \frac{K^{3/2}}{L} \tag{4}$$

is used, which assumes that the rate of dissipation (ε) of turbulent kinetic energy (K) is in equilibrium with the interscale flux of the mean cascade of turbulent kinetic energy. Here L is the integral length scale of the turbulence and C_ε is a constant. (N.B. throughout the manuscript we use standard SI units e.g. L (m), K (m^2/s^2), ε (m^2/s^3) etc.) Henceforth, we refer to this as the *equilibrium* scaling law. More recently, new scaling laws were developed based on the observation that C_ε can in fact be a function of the ratio of two different Reynolds numbers, a global Reynolds number Re_G (defined by inlet conditions) and a local, turbulent Reynolds number Re_L [11] such that $C_\varepsilon \sim Re_G^m / Re_L^n \neq \text{const.}$ This scaling for the dissipation coefficient C_ε violates the classical Richardson-Kolmogorov (equilibrium) phenomenology for the mean cascade of turbulent kinetic energy and is henceforth referred to as the *non-equilibrium* dissipation scaling. If self-similar analysis akin to that of George [10] is conducted with $C_\varepsilon = \text{const.}$ being replaced by the non-equilibrium dissipation scaling law then alternative scalings for the centreline mean velocity deficit and wake width are obtained [11–13]

$$\Delta u_C \sim \left(\frac{x - x_0}{\theta} \right)^{\frac{-2}{3-n}} \left(\frac{l}{\theta} \right)^{\frac{-2n}{3-n}} Re_G^{\frac{2(n-m)}{3-n}} \tag{5}$$

$$r_w \sim \left(\frac{x - x_0}{\theta} \right)^{\frac{1}{3-n}} \left(\frac{l}{\theta} \right)^{\frac{n}{3-n}} Re_G^{\frac{m-n}{3-n}} \tag{6}$$

where θ is the momentum thickness, l is the characteristic length of the wake-generating body, and x_0 is a virtual origin. In turbulent, axisymmetric wakes produced by solid objects it has been observed that $m \approx n \approx 1$ [11]. These values lead to the scalings of $\Delta u_C \sim x^{-1}$ and $r_w \sim x^{1/2}$.

An important feature of the non-equilibrium dissipation theory is that it accommodates different values for m and n to describe wake behaviour in different types of flows. Stein and Kaltenbach [14] postulated that the often-observed linear growth of wind turbine wakes could be explained in terms of the non-equilibrium scaling law when $m \approx n \approx 2$; resulting in the scaling laws of $\Delta u_C \sim x^{-2}$ and $r_w \sim x^1$. They validated this by measuring the wake of a model wind turbine placed in a neutrally-stratified boundary layer flow and found it to be in good agreement with the theory. Table 1 provides an overview of the different theoretical scaling laws for the downstream evolution of r_w and Δu_C according to the equilibrium and non-equilibrium dissipation theories.

Table 1
Overview of the theoretical axial scaling laws for the evolution of turbulent axisymmetric wakes defined by the wake half-width, r_w, and the maximum mean velocity deficit, Δu_C.

Scaling Law	r_w	Δu_C
Equilibrium scaling	$\sim x^{1/3}$	$\sim x^{-2/3}$
Square-root non-equilibrium scaling ($m \approx n \approx 1$)	$\sim x^{1/2}$	$\sim x^{-1}$
Linear non-equilibrium scaling ($m \approx n \approx 2$)	$\sim x^{1}$	$\sim x^{-2}$

The added turbulence in the wake can be similarly analysed for its underlying scaling law. For wind energy applications, the overall level of turbulence in the flow of interest is commonly measured by the turbulence intensity which is defined as $I = u'/U$, where u' is the root-mean-square of the turbulent velocity fluctuations in the flow and U is the mean velocity. As previously noted, the available models for turbine-added turbulence intensity show a wide range of exponents for the axial scaling of $I_+ \sim x^\alpha$ which have not been rigorously derived from any theory of conservation. Stein and Kaltenbach [14] attempted to determine a physically motivated scaling law for turbulence intensity and found that their results suggested this to be $I_+ \sim x^{-1}$ which can be consistently explained through the non-equilibrium dissipation theory with a linear wake growth assumption (i.e., $\frac{dr_w}{dx} = \text{constant}$). The Frandsen model for wake-added turbulence (2) subscribes to this scaling, however as the model predates the development of the scaling law [11], we cannot easily conclude the physical validity of this model by citing an adherence to the non-equilibrium dissipation theory.

A further aspect of modelling turbulence intensity in a turbine array is to consider how the turbulence intensity from multiple overlapping wakes would sum. The cumulative velocity deficit from multiple wakes is commonly calculated by simple summation methods such as linear superposition [15,16] or a sum of squares [17,18]. In regions where multiple turbine wakes interact, we could also expect that other turbulent quantities will sum to a certain degree. This summation is less well explored in the current literature and many wind-farm modelling campaigns only take into account the added turbulence intensity induced by the closest upstream turbine [e.g.16,19] or Method *A* in Table 2. With this assumption, in a wind turbine array with regular

Table 2
Overview of three methods for wake turbulence intensity superposition.

Method *A*	Method *B*	Method *C*
$I_{w,i} = \sqrt{I_\infty^2 + I_{+,i}^2}$	$I_{w,i} = \sqrt{I_\infty^2 + \sum_i^N I_{+,i}^2}$	$I_{w,i} = I_\infty + \sqrt{\sum_i^N I_{+,i}^2}$

spacings, the turbulence intensity at each row becomes a constant value after the 2nd row of turbines. Wessel et al. [20] suggested that alternatively, the cumulative turbulence intensity from multiple wakes can be calculated as illustrated by Method *C* in Table 2. Here, $I_{w,i}$ is the total turbulence intensity behind the ith turbine and N is the number of turbines upstream of the ith turbine. Extending the idea of method C, we can also identify a third possible way to sum the turbulence intensity illustrated by Method *B* in Table 2. Note that unlike the scalings for r_w and Δu_C presented in Table 1 the summation approaches for turbulent intensity do not have a theoretical basis and thus introduce empiricism.

In the present work, porous discs were used as representative wind turbines. Previous experimental campaigns have similarly made use of porous discs to simulate the turbulent wakes of wind turbines [21–23]. As noted in Theunissen et al. [24], in order to maintain dynamic and kinematic similarity to real wind turbines, experiments making use of rotating turbine models require the complex redesign of the blade characteristics to replicate realistic power coefficients. Accordingly, static models provide a more cost and time-effective way to investigate wind farm flows. Theunissen et al. [24] concluded that the disc porosity is the dominant parameter influencing the kinetic energy deficit in the flow. Lignarolo et al. [23] showed that a carefully-designed porous disc model can replicate the wake of a wind turbine to a high degree. While the near-wake ($x/D \lesssim 2$) of a rotating model exhibits significantly higher fluctuations than that of a porous disc, these differences disappear quickly downstream and the wake flow statistics become similar. The experimental campaigns presented in this paper were designed to investigate: (1) the evolution of the turbulent wake from a single representative turbine (porous object), and (2) how turbulent quantities sum when multiple wakes overlap. This paper presents these results with the overarching aim of informing more accurate, and hopefully universally-applicable, wind-turbine wake models with a stronger physical motivation.

2. Experimental methodology

Experiments were conducted in the T1 Wind Tunnel at Imperial College London. The facility is a closed-loop wind tunnel with a test section length of 5 m and a square cross section of 0.914 m × 0.914 m. The experiments were conducted with a uniform inflow of $U_\infty = 10$ m/s and under a freestream turbulence intensity $I_\infty \approx 0.5\%$. The uniformity and low turbulence intensity of the inflow were utilised for this experiment to investigate the turbine-generated turbulence in isolation from the effects of the atmospheric boundary layer and the higher ambient turbulence that would be expected in real-world conditions.

2.1. Porous disc models

The main design parameter of interest for the porous disc models is the porosity, β, which is the ratio between the open and total areas of the disc. The porosity determines the disc's drag coefficient which acts as an analogue for the thrust coefficient of the represented wind turbine, C_T. The disc dimensions were constrained by the desire to keep the total blockage in the wind tunnel below 5% and to prevent their wakes from interacting with the wind-tunnel walls as they spread downstream. Finally, the discs and their towers should be sufficiently stiff to avoid vibrations of the disc free edge and to prevent bending of the tower under the testing wind velocity.

Similar experiments in literature have produced discs with the desired porosity and stiffness by stacking different layers of metal mesh together [23,25], or by using perforated metal plates of specified porosity [26,27]. For this investigation, the decision was made to use perforated plates. Thus, six identical discs of 100 mm diameter were cut from a 1.5 mm-thick sheet of perforated aluminium with a uniform porosity of 45%. The discs were placed along the test section centreline and affixed to towers made of 8 mm steel rods. To facilitate easy adjustment of the spacings between the discs, the models were mounted onto extruded aluminium rails bolted to the tunnel floor. The tower height of $h = 225$ mm avoided submersion of the discs within the boundary layer produced by the rails. Consequently, ground effects are also neglected for this investigation.

The total frontal area of the discs and their respective towers, as well as the mounting rail, resulted in a total blockage of 4.7% in the T1 Wind Tunnel. A disc Reynolds number (based on the disc diameter), Re_D, of approximately 68,500 was achieved at the 10 m/s testing wind velocity — in this regime, the velocity deficit and far-wake turbulence intensity generated by the disc are independent of the Reynolds number [28].

2.2. Experimental procedure

Overall, three runs of experiments were conducted, with the first measuring the wake behind a single disc in order to characterise the individual wake. The next set of experiments then investigated the six discs arranged in a columnar configuration with two different streamwise spacings of $S_x = 5D$ and $3D$, where D is the disc diameter. Whilst a spacing of $3D$ is small in comparison to typical spacings in current wind farms, this test case was deliberately set up to observe the merger of wakes in which the turbulence intensity of multiple wakes from upstream in the array had not decayed to low levels. We also note that with the ever-increasing size of offshore wind turbines in particular, with the largest modern turbines having diameters in excess of 200 m, smaller values of S_x/D will become increasingly common due to space constraints.

Velocity and turbulence measurements were obtained using a single-component, constant temperature anemometry (CTA) hot-wire probe which was mounted onto a computer-controlled 3-axis traverse system. Measurements were taken at the disc centre height ($z = 225$ mm) at $1D$ intervals downstream of each disc for the lateral range of $-1D \leq y \leq 1.5D$ with intervals of $0.1D$. For each measurement point, data was obtained for 30 s at a sampling rate of 10 kHz. A digital low-pass filter with a cut-off frequency of 2.5 kHz was then applied to the raw hot-wire signal before further analysis.

The disc C_T is estimated indirectly through momentum deficit theory and using the velocity deficit distribution downstream of a single disc. Integrating the momentum deficit across the disc area gives an estimate of the axial force acting on the disc [25]

$$T = 2\pi\rho \int_R U_w(r)(U_\infty - U_w(r))y \, \mathrm{d}y \tag{7}$$

where U_w is the mean wake velocity at each radial position and U_∞ is the mean freestream velocity at the disc centre height. This is calculated for the linear-interpolated velocity deficit profile at $x = 3D$ downstream of a single disc where the maximum wake velocity deficit is reached. The disc thrust coefficient is then defined as:

$$C_T = \frac{T}{0.5\rho U_\infty^2 A_D} \tag{8}$$

where A_D is the disc area. Thus, the disc thrust coefficient for an inflow of 10 m/s is determined to be $C_T \approx 0.72$. Whilst inaccuracies in this method are expected, not least due to non-uniform pressure in the measurement region, it is considered satisfactory to produce a representative thrust coefficient

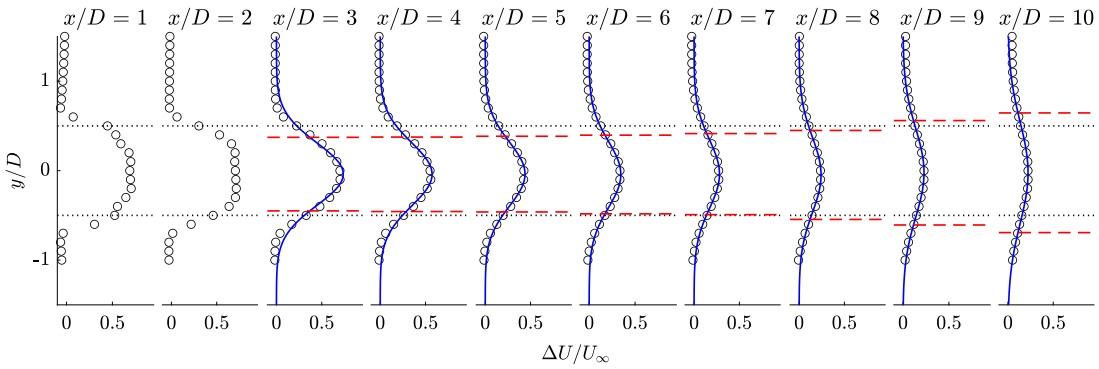

Fig. 1. Lateral profiles of the normalised velocity deficit ($\Delta U/U_\infty$) measured for the single wake at different downstream locations. Solid blue lines depict the profiles' Gaussian fits for the far wake. Dotted black lines mark the disc edges and dashed red lines mark the identified wake edges.

3. Results and analysis

3.1. Single-wake characterisation

Fig. 1 depicts the measured lateral profiles of the normalised mean velocity deficit for the single-wake experiment. A Gaussian function of the form of (9) is fitted to the velocity deficit profiles by way of a nonlinear least squares regression

$$\frac{\Delta U}{U_\infty} = C(x)e^{-\frac{(y-y_c)^2}{2\sigma^2}}. \tag{9}$$

The fitting coefficients are the amplitude coefficient $C(x)$, which corresponds to the maximum velocity deficit in the wake, the standard deviation σ, which defines the characteristic wake width, and the coordinate of the wake centre y_c. The resulting Gaussian fits are depicted in Fig. 1 as the solid blue lines. Observing the quality of the fits suggests that the transition from the near to far-wake occurs at $x \approx 3D$ where the self-similar Gaussian profile becomes a good representation of the wake profile.

According to the wake models proposed by Bastankhah and Porté-Agel [4] and Ishihara and Qian [9], the characteristic wake half-width, $r_{1/2}$, is calculated from the standard deviation of the Gaussian profile as $r_{1/2} = \sigma\sqrt{2\ln 2}$. For a Gaussian distribution, this is also defined as half the lateral distance between two points with a value that is half of the amplitude of the curve (i.e. half of the full width at half maximum). From the coefficients of the Gaussian fit and $r_{1/2}$, the location of the wake edges at each downstream position could also be identified as

$$y^+(x) = y_c(x) + r_{1/2}(x) \tag{10}$$

$$y^-(x) = y_c(x) - r_{1/2}(x) \tag{11}$$

which are depicted by the dashed red lines in Fig. 1. From this, we can observe that the wake expands monotonously from $x/D = 3$ onwards.

The dual-peak profiles of turbulence intensity measured at each location downstream of the single disc are depicted in Fig. 2. The maxima of each profile are found to coincide at or near the disc edges ($y = 0.5D$), consistent with the observations from previous experimental and computational studies of wind-turbine wakes [9,14,29]. A similar procedure to the one performed for the velocity deficit profiles is carried out to fit a two-term Gaussian function (12) to the turbulence intensity profile at each streamwise location

$$I_w = C_1(x)e^{-\frac{(y-y_{c1})^2}{2\sigma_1^2}} + C_2(x)e^{-\frac{(y-y_{c2})^2}{2\sigma_2^2}}. \tag{12}$$

From the resulting fits depicted in Fig. 2, we can observe that the double-Gaussian function provides a good representation of the turbulence intensity profiles, and again shows increasing agreement for $x \gtrsim 3D$. For the double-Gaussian profile, we can define a new characteristic half-width r^* as follows

$$r^* = \frac{\sqrt{2\ln 2}(\sigma_1 + \sigma_2) + |y_{c1} - y_{c2}|}{2} \tag{13}$$

with the location of the wake edges calculated similarly as in (10) and (11), except with the newly-defined wake half-width r^*. Comparing the turbulence intensity profiles to those of the velocity deficit in Fig. 1, we can observe that the wake width as defined by the turbulence intensity profiles is consistently larger than that of the velocity deficit and also expands at a faster rate. Whilst our present data does not enable us to determine the causes for this, one possible explanation is the existence of a ring of intermittent flow that surrounds the wake of a porous disc [30]. Such a ring of intermittency has also been shown to exist in the wake of a realistic wind turbine [31]. With our methodology such an intermittency ring would be detected as elevated turbulence intensity from the low background levels. Further research is, however, required to determine why this intermittency ring spreads at a faster rate than the wake itself as defined by the mean velocity deficit.

The streamwise evolutions of $r_{1/2}$ and r^* are presented in Fig. 3 where the differences in magnitudes and growth rates can be compared. Employing the linear wake growth assumption, linear fits are performed on the data for $x \geq 3D$ to obtain (i) the conventional wake expansion rate k as defined by the growth rate of $r_{1/2}$ for the velocity deficit profile, and (ii) an expansion rate for the turbulence intensity profile defined by the growth of r^*, which we will now denote as k^*.

In the established models for added turbulence in a wind turbine wake, the turbulence intensity distribution is commonly modelled as a constant value across the wake width defined by the velocity deficit profile (i.e. a top-hat distribution) [1,32], or in the case of the model proposed by Ishihara and Qian [9], the turbulence intensity is modelled as a double-Gaussian distribution similar to (12), but with $\sigma_{1,2}$ equal to the value of σ for the single-Gaussian velocity deficit profile. The results presented in this study show that the added turbulence in the wake is not only distributed over a larger spanwise area than the velocity deficit, but that this area also expands at a different rate. Understanding that the turbulence intensity affects the wake characteristics of downstream turbines, we can expect that neglecting these differences can lead to inaccuracies in wind-farm modelling, especially for closely-spaced arrays where the merging of turbulent wakes from multiple turbines would be significant.

3.2. Scaling law analysis of the single-wake case

In Section 3.1, consistent with the established analytical wake models as well as the non-equilibrium scaling law where $m = n = 2$, the wake is assumed to grow linearly downstream. In order to investigate this assumption and compare it against the other theoretical scaling

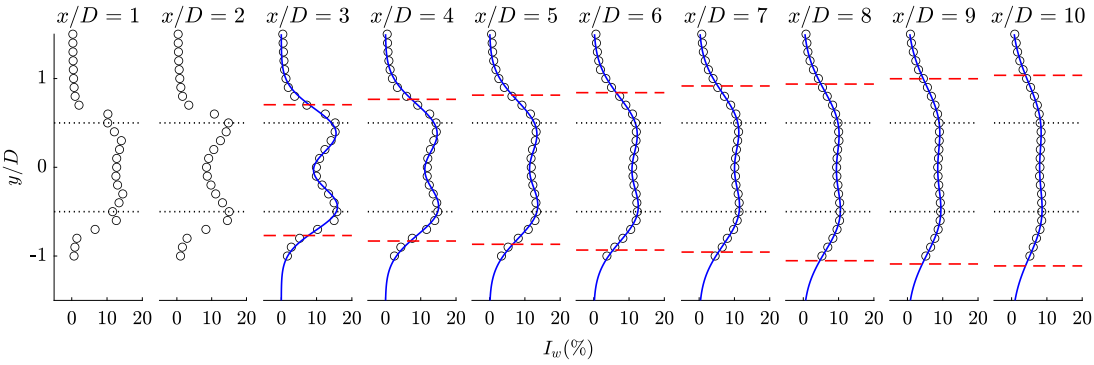

Fig. 2. Lateral profiles of the wake turbulence intensity (I_w) measured for the single wake at different downstream locations. Solid blue lines depict the profiles' double-Gaussian fits for the far wake. Dotted black lines mark the disc edges and dashed red lines mark the identified wake edges.

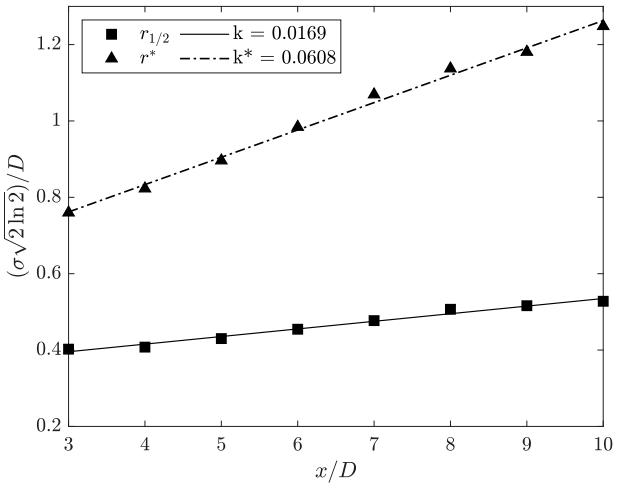

Fig. 3. The downstream evolution of the wake half-width defined by the normalised velocity deficit, $r_{1/2}$, and the half-width defined by the wake turbulence intensity, r^*.

Table 3
The Root-mean-square errors normalised by the range of the measured values (NRMSE), of the power law fits to the measured wake widths, $r_{1/2}$ and r^*, from the single-wake experiment.

Scaling	$r_{1/2}$ NRMSE	r^* NRMSE
$\sim x^{1/3}$	13.2×10^{-2}	8.7×10^{-2}
$\sim x^{1/2}$	6.1×10^{-2}	2.7×10^{-2}
$\sim x^{1}$	5.9×10^{-2}	3.1×10^{-2}

Table 4
The Root-mean-square errors normalised by the range of the measured values (NRMSE) for the power law fits to the normalised maximum velocity deficit ΔU_{max}.

Scaling	ΔU_{max} NRMSE
$\sim x^{-2/3}$	0.171
$\sim x^{-1}$	0.047
$\sim x^{-2}$	0.018

laws laid out in Table 1, power law fits are conducted on the streamwise evolution of $r_{1/2}$ and r^*

$$r_w = b(x - x_0)^{\alpha} \tag{14}$$

where b and x_0 are coefficients to be fitted (x_0 is the virtual origin in (6)), and α is the exponent of the respective scaling laws. The resulting fits are presented in Fig. 4 with the normalised root-mean-square errors (NRMSE) of each fit detailed in Table 3 as a measure of the quality of fit. Immediately, it can be seen that the scaling law of $r_w \sim x^{1/3}$ predicted by the classical equilibrium theory does not provide a good fit to the data. Based on the quality of fit data, we can see that for the experimental conditions of this study, the square-root and linear wake growth scalings are nearly equivalent in their ability to describe the evolution of the conventional wake half-width $r_{1/2}$.

Similar results are obtained for the spreading of the wake width as defined by the turbulence intensity profile; the square-root and linear scalings provide a better fit. This is in contrast to the findings of Stein and Kaltenbach [14] that specifically supported the linear scaling. However, their study only looked at the wake growth in terms of the conventional wake width defined by the standard deviation of the mean velocity profile. It should also be noted that over the relatively small distances typically considered for wind-turbine spacing in a wind farm (i.e. $\lesssim 10D$) Fig. 4(a) shows that there is little difference between the linear and square root scalings. Of course this difference can become large with greater downstream distances and could therefore become significant when computing cumulative turbulence intensity using either Method B or C from Table 2 in large wind farms, or even when estimating the cumulative wake of a large wind farm over several kilometres (which then impinges on a neighbouring wind farm).

The maximum mean velocity deficit in the wake, ΔU_{max} is an important quantity of interest in wind-farm modelling as it determines the wind velocity incident onto downstream turbines which subsequently affects their power output. The theoretical similarity scalings in Table 1 also predict the evolution of the wake centreline mean velocity deficit Δu_C with streamwise distance. For an unyawed wind turbine/porous disc under uniform inflow, this will be equivalent to ΔU_{max}. Similarly to the analysis for the wake-width evolution, the different power laws are fitted to the experimental data and presented in Fig. 5 and the NRMSE of each fit in Table 4. Again, the scaling predicted by the equilibrium theory ($\Delta U_{max} \sim x^{-2/3}$) does not give a good fit to the measured data. For the velocity deficit evolution a larger relative difference is seen between the quality of fits for the square-root and linear scalings with the linear scaling law of $\Delta U_{max} \sim x^{-2}$ providing the better fit of the two.

Given that we are seeking a theoretical basis for the spreading of the turbulent statistics of the wake we should select the best fit for the triplet of $\{r_{1/2}, r^*, \Delta U_{max}\} \sim x^{\{\alpha,\alpha,\gamma\}}$, as opposed to picking and mixing the fits with the lowest NRMSE. Our results therefore suggest at the validity of the linear wake growth assumption in accordance with the non-equilibrium dissipation theory for $m \approx n \approx 2$. Note that the combination of these scalings, i.e. $r_{1/2} \sim x^1$ and $\Delta U_{max} \sim x^{-2}$, is in contrast to the classical Gaussian wake-spreading models in which $r_{1/2} \sim x^1$ and $\Delta U_{max} \sim x^{-1}$ [e.g.4]. By selecting these scalings we are at last able to provide a physics-based rationale for the wake spreading/recovery that does not suffer from inconsistencies such as $r_{1/2}$ and r^* (via I_+)

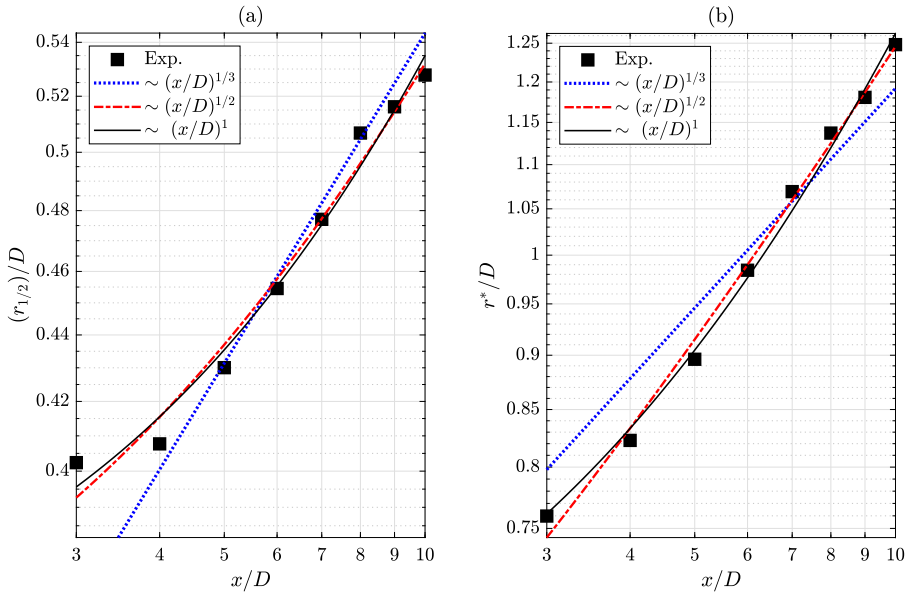

Fig. 4. Power law fits of different theoretical scalings for the streamwise evolution of the measured normalised wake half widths in the far-wake region as defined by (a) the velocity deficit profile and (b) the turbulence intensity profile.

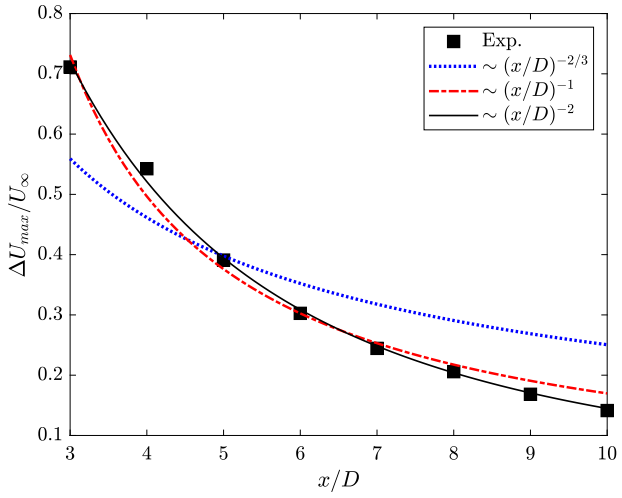

Fig. 5. Power law fits of different theoretical scalings for the streamwise evolution of the measured maximum velocity deficit, ΔU_{max}.

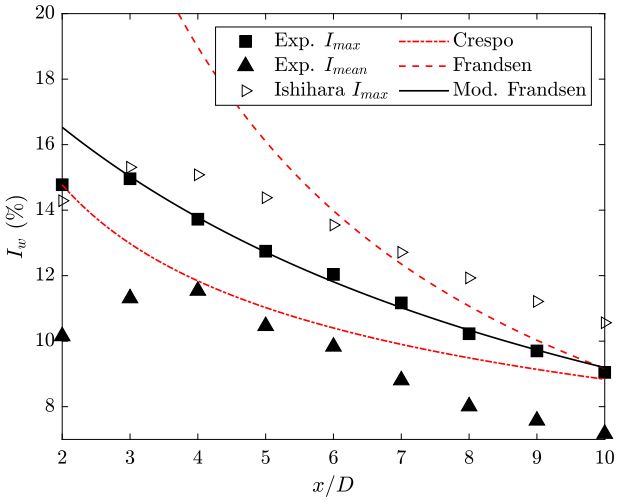

Fig. 6. The maximum and mean turbulence intensities at each downstream station measured in the single-wake experiment (I_{max} and I_{mean}) compared alongside model predictions and a power law fit of the "Modified Frandsen" model function to the I_{max} data.

scaling with (x/D) raised to non-complementary power-law exponents. However, we offer no evidence as to why this is the case with further research being required in this area, in particular why the exponents $m \approx n \approx 2$ for the porous discs we investigate whilst data for wakes produced by non-porous objects suggests $m \approx n \approx 1$ [13]. Further, we note that this physical basis comes at the expense of NRMSE being slightly larger than if we pick and mix scalings for $\{r_{1/2}, r^*, \Delta U_{max}\}$. We have laid out arguments for why it is desirable to have a physical basis for wake spreading (with wind-turbine technology developing rapidly it provides more assurance in extrapolating to newer, bigger turbine designs), however we acknowledge that for our data at least a lower NRMSE across the board can be attained purely empirically.

The streamwise evolution of the maximum turbulence intensity (I_{max}) measured in the wake is depicted in Fig. 6. The mean turbulence intensity, that is averaged across the wake width of $2r^*$, is also plotted against streamwise location. I_+ values predicted by the Crespo and Frandsen added turbulence models are calculated from (1) and (2) respectively. The I_+ maxima of the Ishihara model are also determined as per (3). The total wake turbulence intensities, I_w, for each of these models are then calculated by $I_w = \sqrt{I_\infty^2 + I_+^2}$ where I_0 is the background turbulence intensity in the wind tunnel ($I_0 = 0.5\%$). It is apparent that the Frandsen model substantially over-predicts the wake turbulence from the onset of the far-wake and only falls into decent agreement with the experimental data after $x/D \approx 8$. This could be attributed to the fact that the Frandsen model was developed for the structural design of wind turbines [32] and therefore gives conservative estimations of the wake turbulence. The Crespo model provides better predictions and falls somewhere in between the experimental I_{max} and I_{mean}. However, this model does not accurately represent the trend of the wake turbulence decay. Finally, the Ishihara model consistently over-predicts the maximum wake turbulence (although to a lesser degree than the Frandsen model), however, the trend of its downstream evolution seems to agree well with that of the experimental data.

Motivated by the findings of Stein and Kaltenbach [14] that suggested a physically-motivated axial scaling of $I_+ \sim (x/D)^{-1}$ consistent

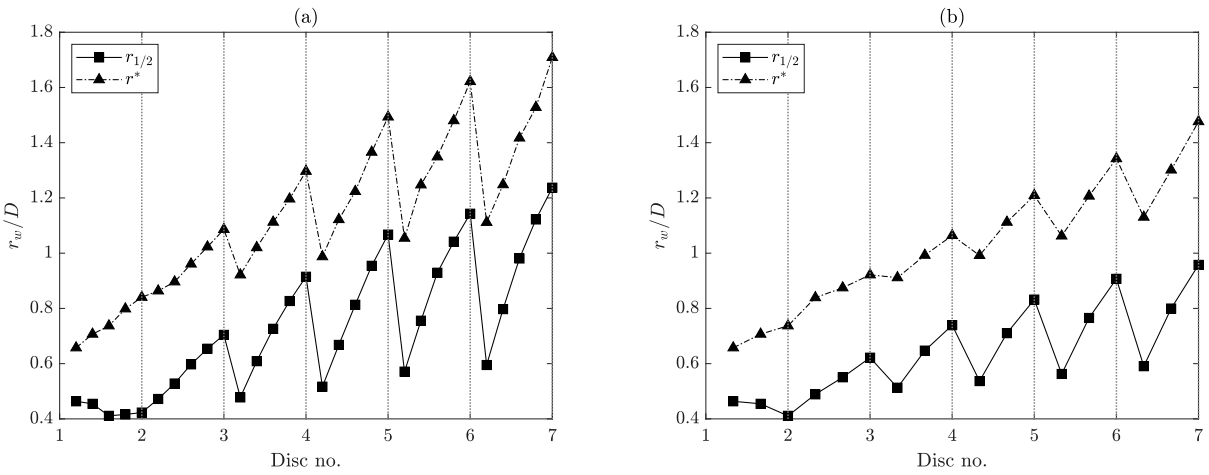

Fig. 7. Streamwise evolution of the normalised characteristic half-widths of the velocity deficit and turbulence intensity profiles ($r_{1/2}/D$ and r^*/D respectively) behind each disc in the one-dimensional array with $5D$ spacing (a) and $3D$ spacing (b).

with the linear wake growth non-equilibrium scaling (under the classical assumption that $u' \sim \Delta U_{max}$), a fit of the Frandsen model function (2) is performed on the experimental values of I_{max} for $x \geq 4D$ to determine new values of c_1 and c_2. This fit can be seen in Fig. 6, denoted as the "Modified Frandsen" model. The resulting function is determined to be:

$$I_+ = \left(5.0 + 0.759\frac{(x/D)}{\sqrt{C_T}}\right)^{-1} \tag{15}$$

Due to the low background turbulence intensity for the experiment, we can assume that (15) gives a good representation of the *added* turbulence intensity due to the disc.

3.3. One-dimensional array experiment

The one-dimensional array experiment had the aim of investigating how turbulence intensities from multiple aligned and overlapping wakes sum. The experiment was performed with six porous discs in a columnar configuration (thus a one-dimensional array). Two different streamwise disc spacings of $S_x = 5D$ and $3D$ were tested in order to explore whether the common assumptions applied in wind-farm modelling hold as turbines are packed closer together. Hot-wire measurements were again taken at $1D$ intervals downstream of each disc. As previously for the single-wake case, Gaussian and double-Gaussian distributions are fitted to the measured velocity deficit and turbulence intensity profiles, respectively.

Fig. 7 presents the two defined wake half-widths plotted against the distance downstream of each disc for both $5D$ and $3D$ cases. Examining the evolution of $r_{1/2}$ in the first wake shows an initially negative trend which is indicative of the very near-wake region. In contrast to this, r^* exhibits monotonous growth immediately behind the first disc. Fig. 7 shows that both $r_{1/2}$ and r^* exhibit drops immediately downstream of a particular disc: this is symptomatic of the way that they are both calculated as Gaussian fitting parameters. Nevertheless, it can be seen that the overall cumulative wake from the array (whether defined as $r_{1/2}$ or r^*) shows the intuitive increasing trend with downstream distance x.

Physically, we picture the wake from a particular disc existing within a turbulent background (produced by the upstream disc-wakes), with each successive wake becoming larger with streamwise distance in response to the increasing influence of the turbulent background. This further illustrates that the spreading of the wake in terms of mean velocity deficit and turbulence intensity behaves differently in the near wake. Keeping the assumption of linear wake growth in the far-wake, the expansion rate behind each disc is determined by a simple linear fitting to the half-width values as a function of x/D to obtain the conventional wake expansion rate k—defined by the spreading of the velocity deficit profile—and the expansion rate of the turbulence intensity profile which we will denote as k^*. The values of k and k^* for the $5D$ and $3D$ spacing cases are detailed in Table 5. As expected, the rate of this wake growth increases with each disc due to the increased turbulence intensity in the "background" of each subsequent row. However, whilst $r^* > r_{1/2}$ for both array spacings it should be noted that, in contrast to the single disc, $k > k^*$, i.e. the wake as defined by the mean velocity deficit grows at a faster rate than that as defined by the turbulence intensity. We postulate that this is due to the definition of the wake as defined by the turbulence intensity becoming increasingly ill defined as the turbulent background (formed from the cumulative effect of all upstream wakes) effectively merges with the outer part of turbulence-intensity-defined wake of a particular disc. These results only go to highlight the complexity of the merging of multiple turbulent wakes in a wind farm.

Table 5
The linear wake growth rates calculated for the wake behind each disc in the 1D array experiment for the $5D$ and $3D$ spacing cases, where k is the growth rate of the velocity deficit profile and k^* is the growth rate of the turbulence intensity profile.

	$5D$ Spacing		$3D$ Spacing	
Disc no.	k	k^*	k	k^*
1	−0.022	0.034	−0.010	0.039
2	0.056	0.035	0.050	0.049
3	0.096	0.065	0.093	0.079
4	0.125	0.092	0.118	0.107
5	0.146	0.119	0.121	0.116
6	0.156	0.147	0.137	0.125

3.3.1. Turbulence intensity superposition

Conventional wind-farm modelling commonly only takes into account the added turbulence due to the closest upstream turbine when determining the turbulence intensity (TI) experienced by a given turbine within an array [e.g.16,19]. For closely-packed wind-turbine arrays, we could hypothesise that this assumption would give rise to more significant errors in predicting the incoming turbulence intensity at a particular turbine and subsequently in modelling its downstream wake characteristics. This can be tested using the results of the array experiment — the values of I_{max} and I_{mean} measured immediately upstream of each disc are extracted and plotted together with the modelled values predicted using the different methods of turbulence intensity superposition as outlined in Table 2. For the sake of this comparison, the added turbulence due to an individual disc is modelled

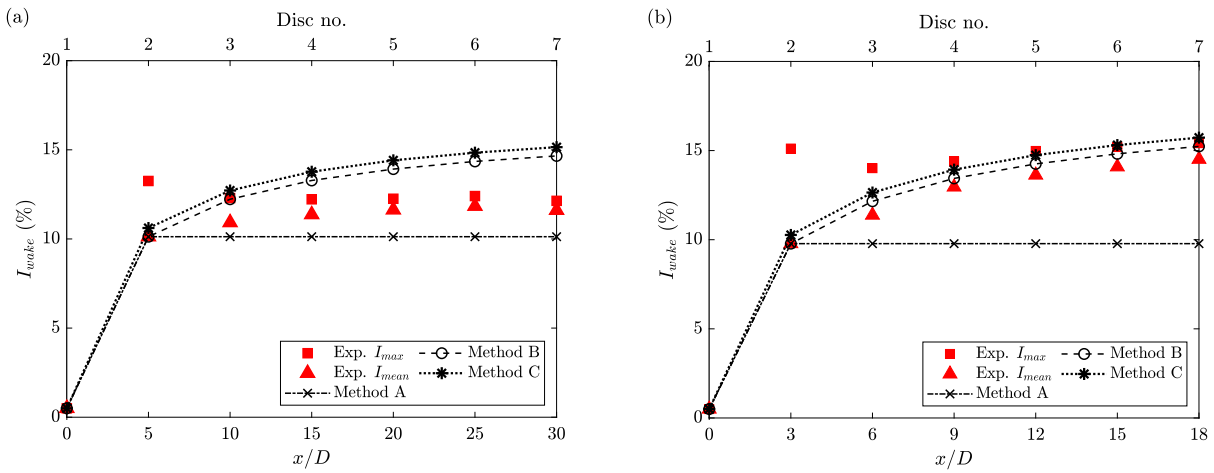

Fig. 8. Experimental maximum and mean turbulence intensity values measured immediately upstream of each disc (red squares and triangles respectively) in the one-dimensional array with spacings of $5D$ (a) and $3D$ (b), plotted with values predicted from the "Modified Frandsen" turbulence model used in conjunction with three methods of turbulence intensity superposition.

by the "Modified Frandsen" model (15) to ensure that deviations are not caused by an over or under-prediction of I_+.

From Fig. 8a we can see that for $S_x = 5D$, Method A under-predicts the TI values at the locations downstream of multiple discs whereas the alternative Methods B and C produce over-predictions of I_w that increasingly deviate from the measured values further downstream. Thus, in the case of $5D$ spacing, Method A is the most appropriate option. In contrast, examining the case where $S_x = 3D$ as seen in Fig. 8b, we can observe that the wake turbulence intensity at each disc location does not reach the asymptotic behaviour that is often seen in wind farms after several turbine rows [19,33]. In this case of small inter-disc spacing, Methods B and C seem to be able to predict the incoming turbulence intensity at each row to a good degree, with Method B giving a slightly better agreement to the measured values. In the closely-spaced array, Method A's underestimation of the wake turbulence intensities is more significant and results in the conventional method showing the poorest agreement with the experimental data between the two cases.

As porous discs are placed closer together, the wake turbulence intensity of upstream discs do not decay sufficiently to maintain the validity of the assumptions of Method A - the cumulative turbulence induced by all upstream discs must be considered in order to produce good turbulence intensity predictions and facilitate accurate wake modelling. Whilst it is unlikely that current wind turbines within a real wind farm will be placed at such short distances apart the lateral spreading of wind turbines in staggered, two-dimensional arrays, are likely to contribute to the cumulative turbulence intensity experienced by a turbine centrally located within a large array. Further, as future wind turbines become ever larger, space constraints on potential wind-farm sites makes smaller S_x/D values increasingly likely. In these cases our results show that it is important to consider this source of additive turbulence when the intersection of the wake and turbine is sufficiently close. Overall, since the alternative Methods B and C were also found to be lacking when applied to the $5D$ case, this points towards the need for the development of a summation method that has a wide range of applicability across different turbine spacings.

4. Summary

In this study, porous discs were used as representative wind turbines in a series of wind tunnel experiments which included studies for a single wake case as well as for an aligned column of six "turbines". The single-wake study established that profiles of turbulence intensity grow downstream at a rate different from that of the mean velocity deficit profile. Furthermore, the turbulence intensity in the wake was also found to be distributed over a larger area than the velocity deficit. These differences could be characterised by defining a separate characteristic wake half-width r^* (13), and wake expansion rate k^*, for the turbulence intensity profile. Today's conventional analytical wake models do not consider these observed differences which becomes a source of inaccuracies that is expected to manifest in more significant errors as we attempt to model larger and more closely-packed wind farms.

The single-wake study also allowed the underlying axial scaling laws for the evolution of the wake widths, velocity deficit, and added turbulence intensity to be investigated. By producing power law fits to the measured data, the scaling laws predicted by the equilibrium and non-equilibrium theories (see Table 1) were assessed. Consistent with the findings in Stein and Kaltenbach [14], the axial scaling laws predicted by the classical equilibrium theory did not produce a good fit to the experimental data. The linear scaling predicted by the non-equilibrium theory where $m = n = 2$ in (5) and (6), proposed by Stein and Kaltenbach [14], was found to provide good fits for the evolution of the conventional wake width $r_{1/2}$ and the maximum mean velocity deficit ΔU_{max}. Furthermore, the linear wake growth scaling also predicts a scaling of $I_+ \sim (x/D)^{-1}$ which is consistent with the Frandsen model for added turbulence intensity (2) under the assumption that $u' \sim \Delta U_{max}$. As the coefficients used in the original Frandsen model produced conservative values for the wake turbulence, a "Modified Frandsen" model was developed by fitting the Frandsen model function to the experimental values which determined new values for the model coefficients as $c_1 = 5.0$ and $c_2 = 0.759$.

The one-dimensional array experiment—where wake measurements were taken for an aligned column of six porous discs with two inter-disc spacings of $S_x = 3D$ and $S_x = 5D$—had the aim of investigating the summation of turbulence intensities from multiple wakes. It was found that for the smaller disc spacing, the wake turbulence intensity at each row does not reach the asymptotic behaviour that is commonly observed in wind farms after several turbine rows. Thus the conventional method of only taking into account the added turbulence due to the closest upstream porous disc (Method A) breaks down for the $3D$ case. Alternative methods of summing the cumulative turbulence intensities were assessed against the experimental results and found to perform better in predicting the turbulence intensity for the $3D$ case, however produced over-predictions of the incoming turbulence intensity at downstream rows. The results from this study point towards there being significant scope for the development of a potentially universally-applicable method of predicting cumulative turbulence intensities within a turbine array through the use of a wake turbulence intensity superposition method with a stronger physical basis.

Ethical standards

The research meets all ethical guidelines, including adherence to the legal requirements of the study country.

CRediT authorship contribution statement

Elizabeth H. Lingkan: Methodology, Data curation, Data visualisation, Writing – original draft. **Oliver R.H. Buxton:** Conceptualization, Writing – original draft.

Declaration of competing interest

The authors declare that they have no known competing financial interests or personal relationships that could have appeared to influence the work reported in this paper.

References

[1] A. Crespo, J. Hernandez, Turbulence characteristics in wind-turbine wakes, J. Wind Eng. Ind. Aerodyn. 61 (1996) 71–85.

[2] L.J. Vermeer, J.N. Sørensen, A. Crespo, Wind turbine wake aerodynamics, Prog. Aerosp. Sci. 39 (6–7) (2003) 467–510.

[3] R.J.A.M. Stevens, C. Meneveau, Flow structure and turbulence in wind farms, Annu. Rev. Fluid Mech. 49 (2017) 311–339.

[4] M. Bastankhah, F. Porté-Agel, A new analytical model for wind-turbine wakes, Renew. Energy 70 (2014) 116–123.

[5] R.J. Barthelmie, K. Hansen, S.T. Frandsen, O. Rathmann, J.G. Schepers, W. Schlez, J. Phillips, K. Rados, A. Zervos, E.S. Politis, P.K. Chaviaropoulos, Modelling and measuring flow and wind turbine wakes in large wind farms offshore, Wind Energy 12 (5) (2009) 431–444.

[6] F. Porté-Agel, M. Bastankhah, S. Shamsoddin, Wind-turbine and wind-farm flows: A review, Bound.-Lay. Meteorol. 174 (1) (2020) 1–59.

[7] M. Wosnik, N. Dufresne, Experimental investigation and similarity solution of the axisymmetric turbulent wake with rotation, in: Proceedings of the ASME 2013 Fluids Engineering Division Summer Meeting, 2013, V01BT12A004.

[8] S. Frandsen, Turbulence and Turbulence-Generated Structural Loading in Wind Turbine Clusters (Ph.D. thesis) Forskningscenter Risoe, 2007, Risoe-R; No. 1188(EN).

[9] T. Ishihara, G.W. Qian, A new Gaussian-based analytical wake model for wind turbines considering ambient turbulence intensities and thrust coefficient effects, J. Wind Eng. Ind. Aerodyn. 177 (2018) 275–292.

[10] W.K. George, The self-preservation of turbulent flows and its relation to the initial conditions and coherent structures, in: Advances in Turbulence, 1989, pp. 39–73.

[11] J.C. Vassilicos, Dissipation in turbulent flows, Annu. Rev. Fluid Mech. 47 (2015) 95–114.

[12] J. Nedi, J.C. Vassilicos, B. Ganapathisubramani, Axisymmetric turbulent wakes with new nonequilibrium similarity scalings, Phys. Rev. Lett. 111 (14) (2013).

[13] T. Dairay, M. Obligado, J.C. Vassilicos, Non-equilibrium scaling laws in axisymmetric turbulent wakes, J. Fluid Mech. 781 (2015) 166–195.

[14] V.P. Stein, H.J. Kaltenbach, Non-equilibrium scaling applied to the wake evolution of a model scale wind turbine, Energies 12 (14) (2019) 2763.

[15] P.B.S. Lissaman, Energy effectiveness of arbitrary arrays of wind turbines, J. Energy 3 (6) (1979) 323–328.

[16] A. Niayifar, F. Porté-Agel, Analytical modeling of wind farms: A new approach for power prediction, Energies 9 (9) (2016) 1–13.

[17] I. Kati, J. Højstrup, N.O. Jensen, A simple model for cluster efficiency, in: EWEC86. Proceedings. Vol. 1, 1987, pp. 407–410.

[18] S. Voutsinas, K. Rados, A. Zervos, On the analysis of wake effects in wind parks, Wind Eng. 14 (4) (1990) 204–219.

[19] P. Argyle, S. Watson, C. Montavon, I. Jones, M. Smith, Modelling turbulence intensity within a large offshore wind farm, Wind Energy 21 (12) (2018) 1329–1343.

[20] A. Wessel, J. Peinke, B. Lange, Modelling turbulence intensities inside wind farms, in: J. Peinke, P. Schaumann, S. Barth (Eds.), Wind Energy, 2007, pp. 253–257.

[21] S. Aubrun, Modelling wind turbine wakes with a porosity concept, in: J. Peinke, P. Schaumann, S. Barth (Eds.), Wind Energy, 2007, pp. 265–269.

[22] J. Bossuyt, M.F. Howland, C. Meneveau, J. Meyers, Measurement of unsteady loading and power output variability in a micro wind farm model in a wind tunnel, Exp. Fluids 58 (1) (2017) 1.

[23] L.E.M. Lignarolo, D. Ragni, C.J. Ferreira, G.J.W. van Bussel, Experimental comparison of a wind-turbine and of an actuator-disc near wake, J. Renew. Sustain. Energy 8 (2) (2016) 023301.

[24] R. Theunissen, P. Housley, C.B. Allen, C. Carey, Experimental verification of computational predictions in power generation variation with layout of offshore wind farms, Wind Energy 18 (10) (2015) 1739–1757.

[25] S. Aubrun, S. Loyer, P.E. Hancock, P. Hayden, Wind turbine wake properties: Comparison between a non-rotating simplified wind turbine model and a rotating model, J. Wind Eng. Ind. Aerodyn. 120 (2013) 1–8.

[26] K. Charmanski, J. Turner, M. Wosnik, Physical model study of the wind turbine array boundary layer, in: Proceedings of the ASME 2014 4th Joint US-European Fluids Engineering Division Summer Meeting Collocated with the ASME 2014 12th International Conference on Nanochannels, Microchannels, and Minichannels, 2014, V01DT39A010.

[27] P.M. Sforza, P. Sheerin, M. Smorto, Three-dimensional wakes of simulated wind turbines, AIAA J. 19 (9) (1981) 1101–1107.

[28] L.P. Chamorro, R.E.A. Arndt, F. Sotiropoulos, Reynolds number dependence of turbulence statistics in the wake of wind turbines, Wind Energy 15 (5) (2012) 733–742.

[29] N.A. Kermani, S.J. Andersen, J.N. Sørensen, W.Z. Shen, Analysis of turbulent wake behind a wind turbine, in: W. Shen (Ed.), Proceedings of the 2013 International Conference on Aerodynamics of Offshore Wind Energy Systems and Wakes, 2013, pp. 53–68.

[30] M.K. Vinnes, I. Neunaber, H-M.H. Lykke, R.J. Hearst, Characterizing porous disk wakes in different turbulent inflow conditions with higher-order statistics, Exp. Fluids 64 (2) (2023) 25.

[31] J. Schottler, J. Bartl, F. Mühle, L. Sætran, J. Peinke, M. Hölling, Wind Energy Sci. 1 (3) 257–273.

[32] S. Frandsen, M.L. Thøgersen, Integrated fatigue loading for wind turbines in wind farms by combining ambient turbulence and wakes, Wind Eng. 23 (6) (1999) 327–339.

[33] L.P. Chamorro, R.E.A. Arndt, F. Sotiropoulos, Turbulent flow properties around a staggered wind farm, Bound.-Lay. Meteorol. 141 (3) (2011) 349–367.